Local Burning Rates and Heat Flux for Forced Flow Boundary-Layer Diffusion Flames

Ajay V. Singh* and Michael J. Gollner†
University of Maryland, College Park, Maryland 20742

DOI: 10.2514/1.J054283

A methodology based on the Reynolds analogy was developed earlier that allowed for the estimation of local mass burning rates and heat fluxes in free-convection laminar boundary-layer diffusion flames. In this study, the relationship was examined in a forced-convective environment using methanol as a liquid fuel. The gas-phase temperature profiles across the laminar boundary layer with a methanol diffusion flame established over it were measured with the freestream air flowing parallel to the condensed fuel surface. Local and averaged mass burning rates were measured along with shear stresses at the fuel surface. The fuel consumption rate and flame lengths were observed to increase monotonically with an increase in the freestream velocity. Although the initial study was taken in the laminar regime, further extensions of the technique could be applicable to turbulent boundary-layer combustion in propulsion-oriented research.

Nomenclature

B	=	B number (Spalding mass transfer number) (–)
C_f	=	local friction coefficient (–)
c_p	=	specific heat at constant pressure, J/kg · K
D	=	species diffusivity, m^2/s
d	=	diameter, m
h	=	convective heat transfer coefficient, $W/m^2 \cdot K$
k	=	thermal conductivity, W/m · K
L	=	length of the condensed fuel surface, m
L_v	=	effective heat of vaporization, J/kg
$\dot{m}_f''$	=	mass burning rate (mass flux), $kg/m^2 \cdot s$
Nu	=	Nusselt number (–)
Pr	=	Prandtl number (–)
$\dot{q}_{\mathrm{fl},c}''$	=	flame convective heat flux, W/m^2
$\dot{q}_{\mathrm{fl},r}''$	=	flame radiative heat flux, W/m^2
$\dot{q}_{\mathrm{net}}''$	=	net heat flux, W/m^2
$\dot{q}_{s,i}''$	=	surface incident heat flux, W/m^2
$\dot{q}_{s,\mathrm{rr}}''$	=	surface reradiation heat flux, W/m^2
T	=	temperature, K
t	=	time, s
U_∞	=	freestream velocity, m/s
X_f	=	flame length, m
x	=	coordinate parallel to condensed fuel surface, m
x^*	=	nondimensional distance, x/L (–)
y	=	coordinate perpendicular to condensed fuel surface, m
y_f	=	flame standoff distance, m
y^*	=	nondimensional distance, y/L (–)
α	=	thermal diffusivity, m^2/s
ε	=	emissivity (–)
ν	=	kinematic viscosity, m^2/s
ρ	=	density, kg/m^3
σ	=	Stefan–Boltzmann constant, 5.67×10^{-8} $W/m^2 \cdot K^4$
τ_s	=	shear stress at the fuel surface, N/m^2

Subscripts

ad	=	adiabatic
tc, b	=	thermocouple junction or bead
f	=	film (mean properties)
fl	=	flame
g	=	gas
p	=	pyrolysis
s	=	surface
w	=	wall/wire
∞	=	ambient

I. Introduction

BOUNDARY-layer combustion has been previously investigated in connection with various applications such as ablative cooling, erosive burning of solid propellants, and surface combustion of liquid fuels. Although there are several studies [1–11] in the literature that have investigated boundary-layer combustion, experimental investigations are limited despite its practical importance. To gain more fundamental knowledge of boundary-layer combustion processes, it is necessary to estimate both local burning rates and incident flame heat fluxes to the condensed fuel surface, because these coupled processes control flame stabilization and thrust for applications such as hybrid rocket propulsion.

The rate of combustion of fuel depends upon mass and heat transfer processes. In a jet or fuel surface combustion, the rate of combustion depends upon the heat and mass transfer processes responsible for heating and evaporating the liquid fuel and diffusing it to meet the oxygen required for combustion [1]. Heat transfer from the reaction zone to the unburnt material has been considered to take place mainly through the gas phase. The amount of heat transferred from the gas phase to the condensed phase depends on the temperature profile in the gas phase adjacent to the combustible surface, and it is closely related to the behavior of gasified fuel, air, and combustion products.

A methodology based on the Reynolds analogy was developed earlier [10,11] that allowed for the estimation of local mass burning rates effectively in free-convective laminar boundary-layer diffusion flames. By extension of the Reynolds analogy, it was hypothesized that the nondimensional temperature gradient at the surface of a condensed fuel is related to the local mass burning rate through some constant of proportionality. This proportionality was tested and verified by conducting experiments in a free-convective environment using methanol and ethanol as liquid fuels and polymethylmethacrylate (PMMA) as a solid fuel, where fine-wire thermocouples were used to get detailed temperature profiles in the vicinity of combustible surfaces [10,11]. The method has its basis in the Chilton–Colburn

Presented as Paper 2015-1386 at the 53rd AIAA Aerospace Sciences Meeting, Kissimmee, FL, 5–9 January 2015; received 5 March 2015; revision received 28 May 2015; accepted for publication 29 May 2015; published online 31 July 2015.

*Graduate Student, Department of Fire Protection Engineering. Member AIAA.

†Assistant Professor, Department of Fire Protection Engineering. Member AIAA.

[12] extension to the Reynolds analogy [13], which establishes a relationship between mass, momentum, and heat transfer in a boundary layer over a solid or liquid fuel surface:

$$\frac{\tau_s}{U_\infty \nu^{2/3}} \equiv \frac{h}{c_p \alpha^{2/3}} \equiv \frac{\dot{m}''}{D^{2/3}\,\ell_n(1+B)} \tag{1}$$

Emmons hypothesized that the shear stress at the surface of a combusting fuel must be proportional to the mass burning rate [1]. Using Eq. (1), the Emmons hypothesis [outlined in Eq. (5)], and a heat transfer coefficient at the surface of a flat fuel [11], an expression for the local mass burning rate can be derived. By extension of the Reynolds analogy, it was hypothesized that the nondimensional temperature gradient at the surface of a condensed fuel is related to the local mass burning rate through some constant of proportionality [11] and is given by

$$\dot{m}_f'' = \frac{C}{L}\left(\frac{\partial T^*}{\partial y^*}\right)_{y^*=0} = \frac{Bk_w}{c_p L}\left(\frac{\partial T^*}{\partial y^*}\right)_{y^*=0} \tag{2}$$

where $T^* = (T - T_{w,p}/T_{\mathrm{fl,ad}} - T_{w,p})$ represents the nondimensional temperature; $T_{w,p}$ and $T_{\mathrm{fl,ad}}$ represent the wall (taken as the pyrolysis temperature of the given fuel) and adiabatic flame temperature, respectively, for a given fuel; L is a length scale representing the length of the region that is pyrolyzing or vaporizing; and $y^* = (y/L)$ denotes the nondimensional normal direction with reference to the surface that is issuing fuel vapor. The definition of the nondimensional temperature was chosen so that the boundary-layer equations can be properly normalized. Also, defining T^* in the manner outlined earlier helps in making the relationship universally applicable over a wide range of fuels and geometry. The proportionality constant C appearing in Eq. (2) equals (Bk_w/c_p), where k_w is the thermal conductivity of the gas phase evaluated at the wall temperature and c_p is the specific heat measured at the adiabatic flame temperature of the given fuel. The term B that appears in Eqs. (1) and (2) is a nondimensional proportionality constant that relates the rate of mass transfer (e.g., vaporization, combustion) to the rate of heat transfer and is essentially the driving force for mass transfer; it was first referred to as the "transfer number" by Spalding [14]. The Prandtl number Pr is assumed to be equal to unity.

The aim of the present study is to use the preceding relationship [defined in Eq. (2)] for estimation of local mass burning rates and flame heat fluxes. Temperature profiles across the boundary layer with a diffusion flame established over a liquid fuel (methanol) with a freestream of air parallel to the combustible surface was measured by using fine-wire thermocouples at four different freestream velocities, namely, $U_\infty = 0.79$, 0.99, 1.54, and 2.06 m/s, respectively. Time-averaged fuel consumption rates were also measured by using a load cell. The relationship described earlier has been further used to separate the convective and radiative components of flame heat flux by carrying out an energy balance at the surface of the liquid fuel. The aim of the present study is to improve the accuracy and predictive capability of numerical models by providing an experimental data set for local burning rates and various components of incident flame heat flux to the condensed fuel surface. Although the initial study was carried out in the laminar regime, further extensions of the technique could be applicable to turbulent boundary-layer combustion.

II. Literature Review

The physical nature of steady, laminar diffusion flames sustained on condensed fuel surfaces have been investigated by a number of researchers in the past. Burke and Schumann [15] were among the earliest researchers to present a theoretical analysis of a general diffusion flame from homogeneous reactants. They solved the problem of flame zone in concentric duct burners with a gaseous fuel flowing in the core and air flowing in the annular regions. Spalding [16] addressed the problem of fuel pyrolysis due to energy transfer from a combustion zone. The modern era of studies on diffusion flame, with application to fire safety, began with the pioneering work on mathematical modeling of steady flame carried out by Emmons [1]. A similarity solution of the classical reacting boundary-layer problem under a zero-gravity environment was reported. An analytical expression for the burning rate of a diffusion flame established over a horizontal liquid fuel surface that was subjected to forced airflow parallel to its surface was proposed. Emmons, in his analysis, established the foundations for the theoretical modeling of this problem. Using the boundary-layer and flame sheet approximations, he obtained explicit formulas for the mass burning rate in terms of the gas flow parameters and fuel properties. Because of the simplicity of the closed-form equation, the Emmons classical solution was used widely and provided a starting point for flame propagation studies carried out subsequently by Kosdon et al. [2], Kim et al. [3], Pagni and Shih [6], and Annamalai and Sibulkin [8]. Kosdon et al. [2] and Kim et al. [3] applied the same methodology to develop analyses of the laminar free-convective burning of a vertical fuel surface, and they conducted experiments that verified the mass burning rate predictions of the model. Much later, Pagni [17] presented a review of various aspects of classical diffusion flames relevant to fire safety. He explored, among others, problems involving forced, free, mixed, and stagnation point combusting boundary layers. Several research studies reported the use of boundary-layer assumptions to describe fire-related parameters such as the flame length [6], flame spread rate [8], and flame standoff distance [18]. Extensive reviews on the application of the Emmons model [1], to predict laminar flame propagation on liquid and solid fuel surfaces, are also found in the works of Sirignano [19] and Williams [20].

Experimental studies followed analytical work, investigating various aspects of nonspreading, steady boundary-layer-type diffusion flames. One of the earliest experimental investigations on the aerodynamic structure and stability of diffusion flames stabilized over a fuel surface was reported by Hirano et al. [4,5], where gaseous fuels were injected uniformly through a porous flat plate into a parallel airstream. These experiments showed that the aerodynamic structure of the boundary layer is significantly different in the presence of a diffusion flame when compared with the boundary layer without a flame. Both velocity as well as temperature profiles were obtained at various locations along the plate surface. In their subsequent experimental studies, Hirano and Kinoshita [21] measured gas velocities and temperature profiles across a diffusion flame established over a liquid fuel surface with a free airstream parallel to the plate. Later, Andreussi and Petarca [9] carried out experiments similar to those by Hirano and Kinoshita [21] using ethyl alcohol as a fuel. These authors studied the structure of the diffusion flame formed on a liquid surface with a parallel oxidizer flow experimentally, analytically, or both. Andreussi [22] later developed a theoretical model based on the Shcvab–Zeldovich formulation of the problem. In a subsequent study, Andreotti et al. [23] completed the analysis of boundary-layer diffusion flames with measurements of velocity profiles, fuel-burning rates, and temperature profiles over a wide range of conditions for various liquid fuels. Gas velocity and temperature profiles were measured by Hirano and Kinoshita [21], whereas Andreussi and Petarca [9] measured the temperature, velocity, and species concentration profiles across the boundary-layer diffusion flame. However, previous studies did not measure the local temperature gradients at the surface of a condensed fuel and no attempt was made to measure the local fuel consumption rate. A recent study by Singh and Gollner [10,11] used a first set of temperature measurements close to the fuel surface of buoyant methanol, ethanol, and PMMA wall flames to calculate the local mass burning rates by using a new technique based on Eq. (2).

III. Experimental Facility and Instrumentation

Figure 1 is a schematic of the experimental setup, the key components of which include a wind tunnel, fuel wick holder, and thermocouples mounted on a set of Velmex X-Y unislides. The wind tunnel has a $100 \times 75 \times 100$ cm plenum at one end, into which an Ebm papst (G3G250-MW72-01) variable-speed blower pressurizes the air. This pressure buildup in the plenum drives the flow of the air through the wind tunnel; hence, the effects of the blower on the flow

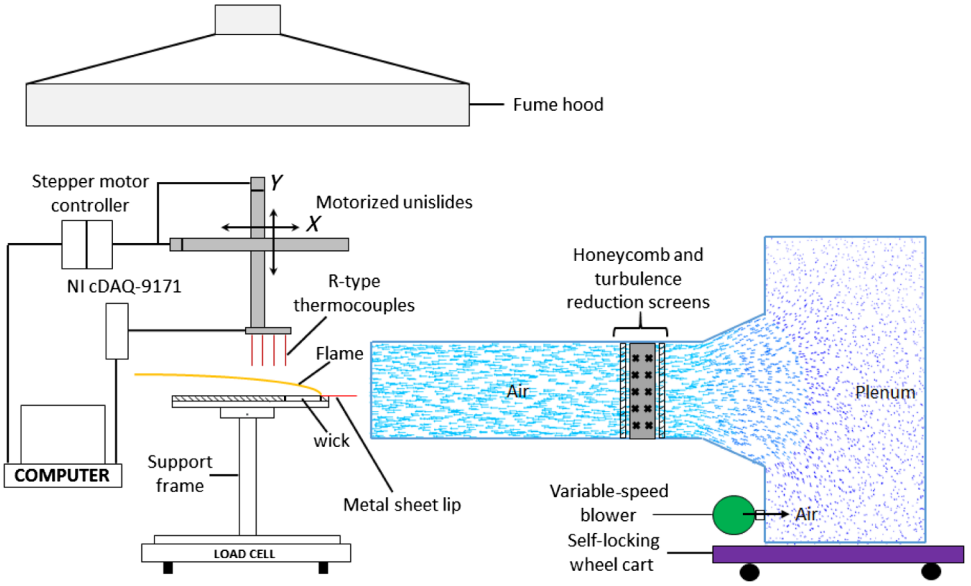

Fig. 1 Schematic diagram of experimental setup used to measure mass loss rates and temperature profiles over a forced-convection boundary-layer diffusion flame.

are minimized. A 30.48 cm converging section connects the plenum to the 122 cm straight section, which has a 30.48 × 30.48 cm cross section. A set of fine screens are placed at the entrance and exit of the converging section and a combination of turbulence reduction screens and 5-cm-thick honeycomb with 0.3-cm-diam holes is inserted 110 cm upstream from the tunnel exit to straighten the flow. The flow velocity in the wind tunnel is selected by adjusting the speed of the blower with the help of a pulse-width-modulation controller. The fuel-soaked wick is positioned outside the wind tunnel, at the center of the tunnel exit. This makes it easier for the thermocouples to be moved freely in and out of the flame to measure the gas-phase temperatures.

The sample holder sits on a load cell and consists of two U-shaped aluminum brackets, which were connected to an aluminum sheet (measuring 30.48 × 60.96 cm and 1.5 mm thick) and mounted vertically atop a load cell. A sheet of ceramic fiber insulation board 1.27 cm thick, with a section 2 cm from the base of the sheet cut out for holding the fuel sample, was mounted atop the aluminum sheet. A thin metal lip measuring 40.64 × 10 cm was attached just before the leading section of the condensed fuel surface to reduce the flow separation and bluff-body effects of the sample holder and to prevent the transition of a laminar boundary layer due to surface roughness of the upstream insulation board. According to Ha et al. [24], by attaching an extension plate at the leading edge of the fuel surface, the separation of flow may be prevented and an ordinary boundary-layer diffusion flame can be established. In the flow without an extension plate, the interaction between the flow separation and the diffusion flame was found to exist [24]. Therefore, our condensed fuel surface starts 10 cm away from the exit of the wind tunnel. At the measurement location, the holder is positioned with its leading edge against the wind-tunnel exit at the center of the channel. Because the metal sheet lip is wider (40.64 cm) than the width of the tunnel (30.48 cm), the exiting air jet is divided into two and the top half forms a boundary layer over the sample. The front surface of the insulation wall was coated with a black radiation-absorbing paint having an absorptivity of approximately 98%. The liquid fuel wick was a 10 × 10 × 1.27-cm-thick sheet of porous noncombustible material (alkaline earth silicate wool). To eliminate leakage of the liquid fuel from the sides, sodium silicate was applied to all interfaces of the wick except the top face. Burning was limited to the front surface of the wick by shielding the remaining sides with aluminum foil. During testing, the wick was soaked with liquid fuel up to its point of saturation so that it gave a stable boundary-layer diffusion flame for the longest time duration possible (enough to take precise temperature measurements). The fuel wick was soaked with approximately 120 ml of liquid fuel for each test.

The fuel burning rate was measured by monitoring the mass loss of the burning wick over a timed interval. A Mettler Toledo precision mass balance was used, which had a maximum capacity of 32.2 kg and a resolution of 0.1 g, to measure the mass loss rate of the condensed fuel surface. The average mass loss rate of the condensed fuel surface was determined by measuring the slope of the linear mass loss versus time curve during steady burning. The burning rate measurements presented are averages of six tests at a given condition. The repeatability of these measurements was within 1.2% of the mean.

Precise temperature measurements were carried out using *R*-type Pt/Pt-13% Rh microthermocouples (spot welded) of 50 μm (0.002 in.) and 75 μm (0.003 in.) wire diameter with a bead of approximately 100 and 150 μm in diameter, respectively (according to manufacturer's specifications). In practice, most thermocouples have bead diameters in the range $1.5\,d_w < d_b < 2.5\,d_w$ (in our case, $d_b \sim 2d_w$). The microthermocouple wires were housed in a single 1.1-mm-diam twin bore ceramic cylinder and a smaller length of thermocouple wire was exposed. Microthermocouples were mounted to a set of computer-controlled Velmex X-Y unislides such that they could be moved precisely up and down along the flame length or left and right across the flame thickness, with a maximum spatial resolution of 1.5 μm. Voltage signals from the thermocouples were acquired, conditioned, and digitized through a National Instruments NI 9214, which is a 24 bit high-density 16 channel thermocouple input module that can be used up to 0.02°C measurement sensitivity. The LabVIEW software was used for synchronized motor control and continuous temperature data acquisition. Both 50 and 75 μm wire diameter thermocouples were used over the same sample to ensure accurate radiation corrections by reading the difference between these two at the same location and applying the correlation of Collis and Williams [25]. For the 50 μm wire diameter thermocouple, a typical radiation correction at 1700 K was found to be approximately +79 K. Because the thermocouples cross regions of high-temperature gradients, the measurements are expected to include conduction errors, however, they have been estimated to be small here (<1%) because the heat transfer area (the cross section of the thermocouple) is very small, therefore no corrections were made in the data for conduction errors.

Measurements of the flame standoff distances were recorded by digital photographs, where the distance from the condensed-fuel surface to the center of the blue flame zone was measured and taken as the position of the flame. The flames were photographed in a darkened room with a side-view digital camera (Canon EOS). Before a sample was ignited, the camera was calibrated by taking a picture of a sheet of graph paper that was aligned along the horizontal axis of the

fuel surface. The field of view was chosen to reduce errors in the standoff distance measurement to less than 4%. The digital images were averaged in MATLAB and flame standoff distances were measured by using ImageJ software. In a particular test, 200 images were averaged during the steady burning regime time to obtain an averaged image. Flame standoff measurements were carried out independently for three repeated tests at a given flow condition. The results were then averaged to give an averaged flame standoff distance profile. The repeatability of these measurements was within 2% of the mean.

Generally, in forced-flow boundary-layer flame experiments, the fuel sample is placed inside a wind tunnel. In this work, we placed the condensed fuel surface at the exit of the wind tunnel in the center of the airstream. This arrangement enabled us to obtain easy access to the boundary-layer flame and condensed fuel surface for temperature and flow characterization. The wind tunnel was fully characterized for different blower speeds and velocity profiles and turbulence intensity levels were measured at the wind tunnel outlet using a Dantec Dynamics hot-wire anemometer. The freestream velocity U_∞ was then calculated by integrating the obtained velocity profile at the tunnel outlet. The velocity data at each point were acquired with a sampling rate of 50,000 samples/s for a total duration of 10 s. The repeatability of these measurements was within 3% of the mean. The velocity profile across the tunnel outlet was found to be relatively uniform near the center. Figure 2a shows the velocity profiles obtained at the wind-tunnel outlet for four different blower speeds. To ensure that the flow is well defined at the location of the flame, we chose the dimensions of the sample to be small such that the condensed fuel surface would be within the potential flow core of the exit jet. It has been shown that velocity profiles in both x and y directions do not change significantly within the potential core of the jet [26,27]. Experimental measurements from Sforza et al. [28] show that, for an air jet at the exit of a square channel, with Reynolds number Re_d between 2.6 and 8.8×10^4, the potential flow core length is about $5d$ downstream of the exit, where d is the height of the channel. In the current work, $d = 30.48$ cm and hence our sample is within $1d$ (20 cm from the tunnel exit). Our Re_d is between 1.5×10^4 and 3.9×10^4; therefore, the flame would be within the potential flow core of the jet. To further confirm that the velocity profiles would not change significantly within the space where the flame would exist, the velocity profiles were measured above the nonburning sample. Figure 2b shows the variation of inlet velocity within the potential core of the exit jet with the streamwise distance x from the leading edge of the sample holder surface. Figure 2b shows results for heights of 32, 35, and 40 mm above the sample surface at three distinct streamwise locations. The thermal boundary-layer thickness at the trailing edge of the sample is approximately 30 mm for $U_\infty =$ 0.79 m/s. Figure 2b shows that the velocity profiles have not changed significantly within the core space where the flame is located.

During the experimental tests, the data acquisition system acquired temperatures at 500 samples/s, providing 500 samples to average per spatial point. Reported temperatures are averages of at least five tests in a given condition and the maximum standard deviation was <3.2% of the mean. The inherent uncertainty in temperatures measured by the thermocouple T_{tc} are taken to be 0.25% of the measured value based on manufacturer's specifications. The accuracy of the Nusselt number correlation used to calculate the radiation loss from the thermocouple bead was reported to be within 5% [25] and the uncertainty in k due to different species is assumed to be 3%. The error in the thermocouple emissivity ε_{tc} used is also small, $< \pm 3\%$, except that ε_{tc} is linear with T_{tc}, and so any error in T_{tc} increases the uncertainty in ε_{tc}. The platinum emissivity was calculated using Jakob's theoretical correlation [29], confirmed by experimental data of Gubareff et al. [30], which reported the Pt emissivity uncertainty $< \pm 3\%$ when using the calculation. The uncertainty in gas temperature is then calculated from a quadratic sum of the uncertainties

$$dT_g = \left[\left(\frac{\partial T_g}{\partial T_{tc}} dT_{tc}\right)^2 + \left(\frac{\partial T_g}{\partial \varepsilon_{tc}} d\varepsilon_{tc}\right)^2 + \left(\frac{\partial T_g}{\partial k} dk\right)^2 + \left(\frac{\partial T_g}{\partial Nu} dNu\right)^2\right]^{1/2} \quad (3)$$

The maximum uncertainty in gas temperatures encountered in the flame zone is then found to be within ± 7 K. The maximum expanded uncertainty in gas temperatures is then found to be within ± 14 K with a 95% confidence interval.

IV. Results and Discussion

A. Boundary-Layer Diffusion Flames Under Forced Flow

For an appropriate value of uniform airstream velocity U_∞, a stable, laminar two-dimensional diffusion flame could be established over a condensed fuel surface. When U_∞ was increased above the stability limit ($U_\infty > 2.2$ m/s), the leading flame edge became unstable and local quenching of the flame was observed at the leading edge of the fuel surface. Increasing the flow velocities further blew off the flame completely. These limits of stability were previously investigated by Raghavan et al. who used numerical simulations to determine the range of Reynolds numbers under which the Emmons solution is valid [31]. Within this stable regime, the flame anchors near the leading edge of the condensed fuel surface and the combustion zone is confined beneath the hydrodynamic and thermal

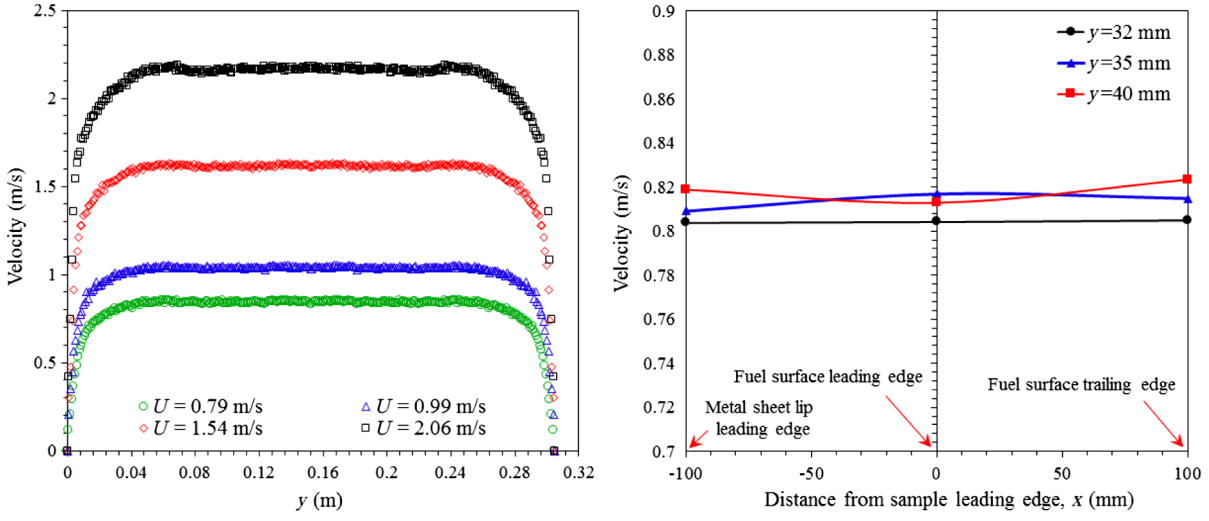

Fig. 2 Depiction of a) velocity profiles at wind-tunnel outlet for different blower speeds; and b) streamwise variation of air velocity beyond the tunnel exit.

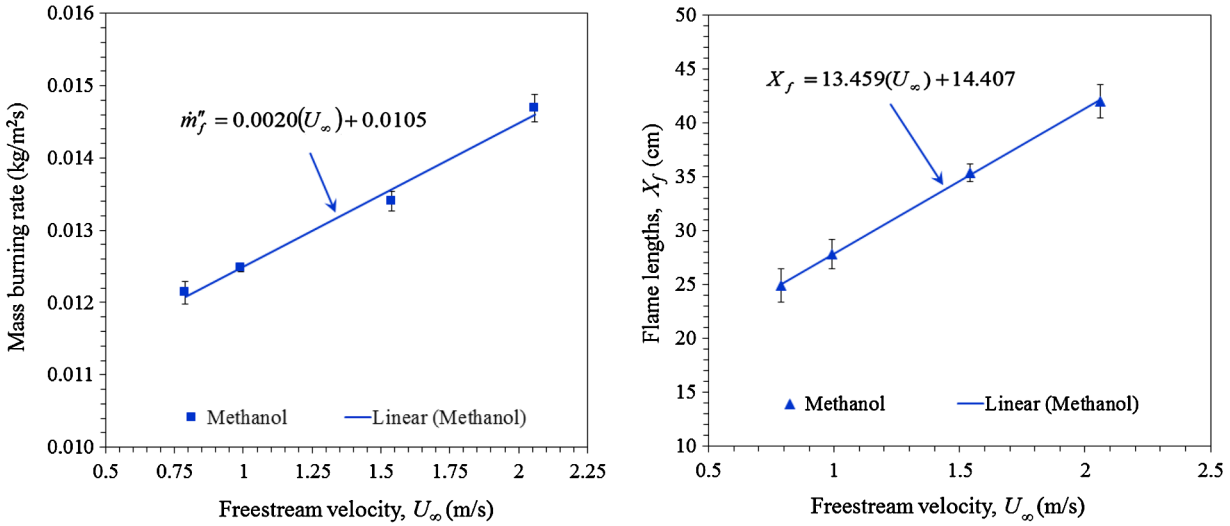

Fig. 3 Averaged mass burning rates (left) and flame lengths (right) for a methanol boundary-layer diffusion flame.

boundary layers. However, in the case of very low freestream velocities, the combustion zone is beyond the boundary layer, and in cases of very high freestream velocities, the flame moves away from the leading edge and anchors at a location downstream, invalidating the Emmons solution in these regimes [31]. In the present work, freestream velocities were carefully chosen in the range where the Emmons solution is valid.

The flame standoff distance was found to increase with the distance x from the leading edge. As U_∞ is increased, the flame approaches the condensed fuel surface and the flame anchoring distance was found to shift downstream. The luminosity of the blue flame zone decreased as x increased. The averaged mass burning rates and flame lengths were observed to increase monotonically with an increase of U_∞. Figure 3 shows the comparison of averaged mass burning rates and flame lengths for a methanol boundary-layer diffusion flame established under different freestream velocities. Figure 4 shows the side-view direct flame photographs of a methanol boundary-layer diffusion flame at freestream velocities of 0.79 and 2.06 m/s, respectively.

B. Gas-Phase Temperature Profiles

Using the experimental apparatus described earlier, measurements were taken for local temperature profiles along condensed fuel surfaces. Figure 5 shows the temperature profiles at several streamwise locations along the condensed fuel surface for a methanol boundary-layer diffusion flame at freestream velocities of 0.79 and 2.06 m/s, respectively.

On the downstream side of the leading flame edge, T increases with y to a maximum flame temperature T_{fl} at the flame zone. On the airstream side of the flame zone, T decreases with y to ambient temperature at the thermal boundary-layer edge. T_{fl} at a given streamwise location was found to increase slightly with an increase in U_∞. Within about 2–3 cm of the leading edge of the condensed fuel surface, T_{fl} increases in the x direction. Further downstream, T_{fl} decreases in the x direction. The same observations were made by Hirano et al. [4] when they studied ethanol and methanol diffusion flames in a forced-convective environment. The peak flame temperature was found to be 1906 and 1980 K for $U_\infty = 0.79$ and 2.06 m/s, respectively. At the trailing edge of the sample, the peak flame temperature drops by about 186 and 219 K for freestream velocities of 0.79 and 2.06 m/s, respectively. This temperature decrease is primarily due to convective heat losses. The temperature of the condensed fuel surface was found to be approximately near the boiling point of methanol at different forced-flow conditions. Observation of the temperature gradients normal to the fuel surface suggests that they are highest near the leading edge and decrease further downstream. The temperature gradient $(\partial T/\partial y)_0$ at $y = 0$ decreases in the x direction downstream of the leading edge. The $(\partial T/\partial y)_0$ at a given streamwise location was found to increase with an increase in U_∞. This is consistent with known characteristics of boundary-layer diffusion flames, in that convective heat feedback decreases with x for a particular U_∞ and increases at a given streamwise location with an increase in U_∞. The local mass loss rate from the fuel, driven by convective heat fluxes to the surface in these small laminar flames, should similarly decrease with x. The flame usually becomes thicker when moving downstream of the leading edge and the flame standoff distance increases with increasing x. It follows, therefore, that the local mass burning rate should also decrease with x, as discussed later.

C. Flame Standoff Distance and Nondimensional Temperature Gradients

The flame standoff distance y_f at different locations along the fuel surface are plotted in Fig. 6a for a methanol boundary-layer diffusion flame established under freestream velocities of 0.79, 0.99, 1.54, and 2.06 m/s, respectively. The flame standoff distance is lower near the

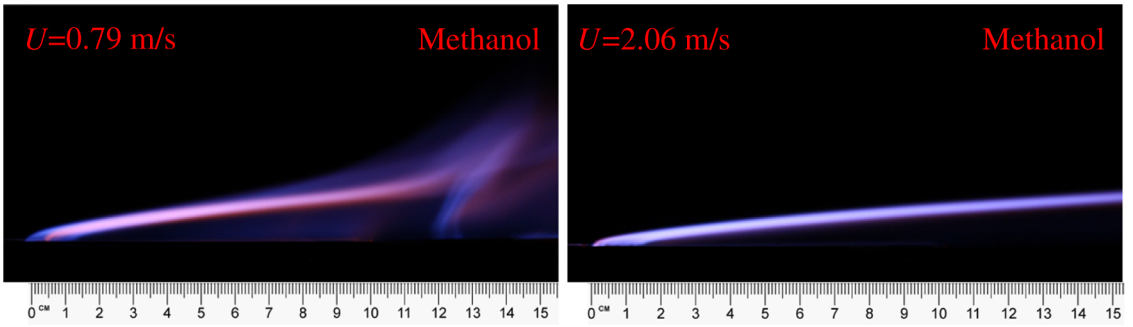

Fig. 4 Side-view photograph of methanol boundary-layer diffusion flame at $U_\infty = 0.79$ and 2.06 m/s, respectively.

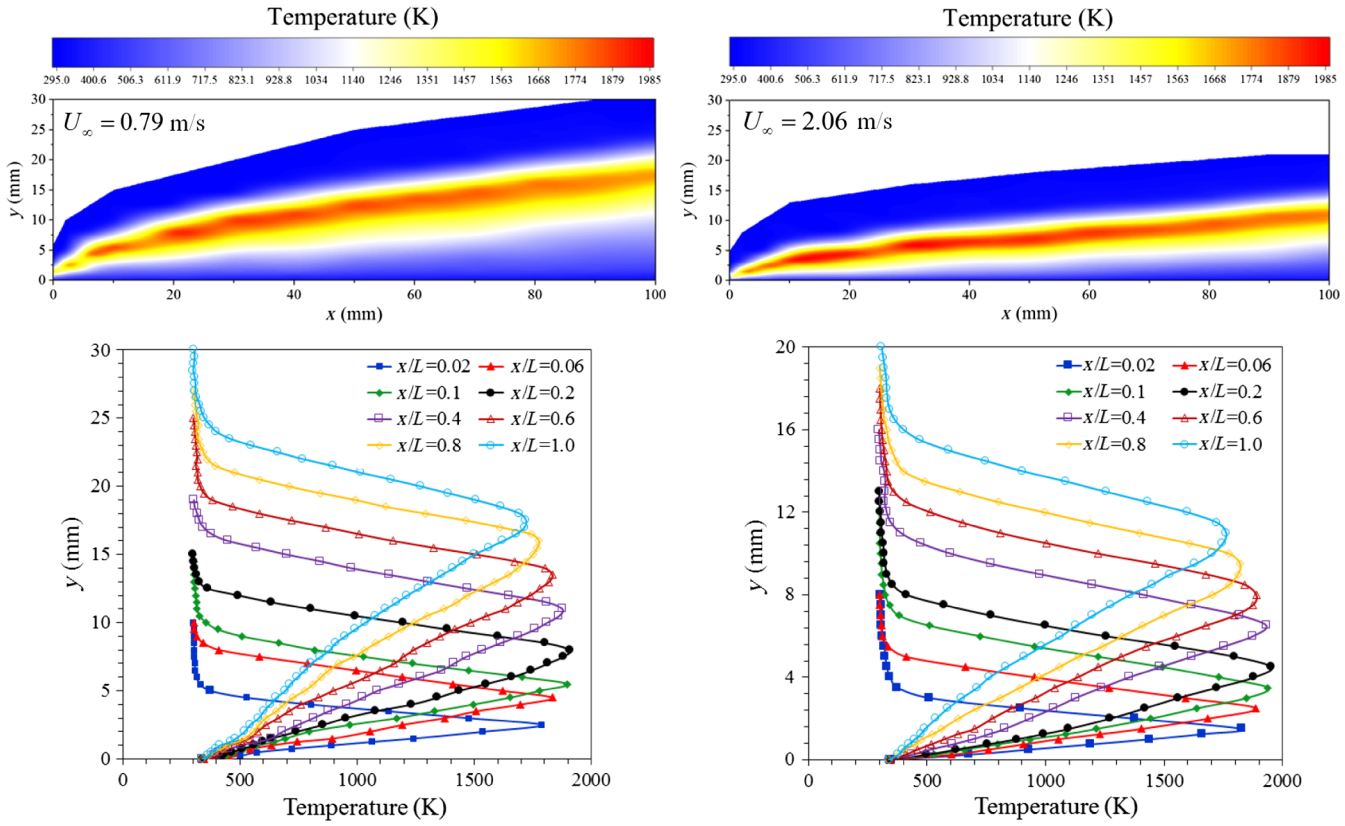

Fig. 5 Gas-phase temperature contours and profiles for a methanol boundary-layer diffusion flame at (left) $U_\infty = 0.79$ and (right) $U_\infty = 2.06$ m/s.

leading edge and it increases further downstream up to the trailing edge. This leads to enhanced heat transfer to the fuel surface at the leading edge and hence higher evaporation rates of the fuel at this location. Accordingly, the local burning rate is highest at this location. The flame standoff distance is higher for the regions near the trailing edge and hence heat transfer at these locations is lower. Because of lower heat transfer rates at these locations, the local mass burning rates are found to be lower at these locations. Also, the flame standoff distance is almost proportional to $x^{0.5}$, confirming the similarity theory for a forced-convection boundary layer adjacent to a horizontal flat plate [1,32]. As U_∞ is increased, the flame approaches the condensed fuel surface and the flame anchoring distance was found to shift downstream.

Figure 6b shows the variation of the normal nondimensional temperature gradient along the fuel surface extracted from experimental temperature data of a methanol diffusion flame for $U_\infty = 0.79$ and 2.06 m/s. The normal nondimensional temperature gradients at the fuel surface $(\partial T^*/\partial y^*)|_{y^*=0}$ were calculated from the slope at $y^* = 0$ of a fifth-order polynomial fit to the nondimensional temperature distribution near the fuel surface. The temperature gradient normal to the fuel surface was found to be highest at the leading edge and lowest at the trailing edge ($x = 100$ mm). The local mass burning rate should follow a similar trend, as is revealed by the calculated rates in Fig. 7.

Averaging the nondimensional temperature gradient for the entire fuel surface, the average mass burning rate is estimated to be 12.38,

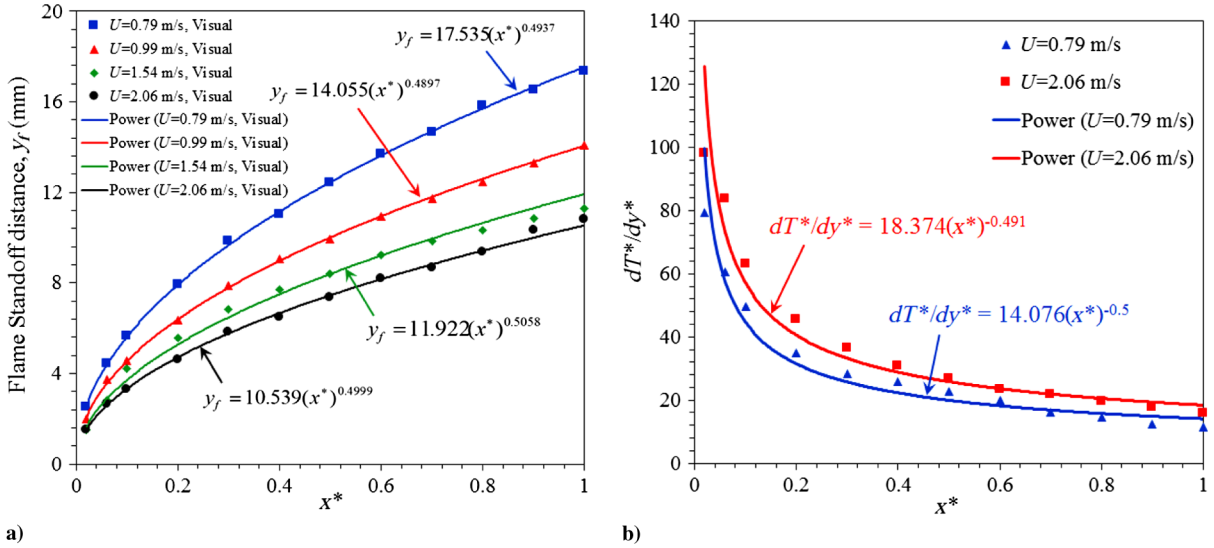

a) b)

Fig. 6 Depiction of a) variation of flame standoff distance for different values of U_∞; and b) nondimensional temperature gradients at methanol condensed fuel surface for $U_\infty = 0.79$ and 2.06 m/s.

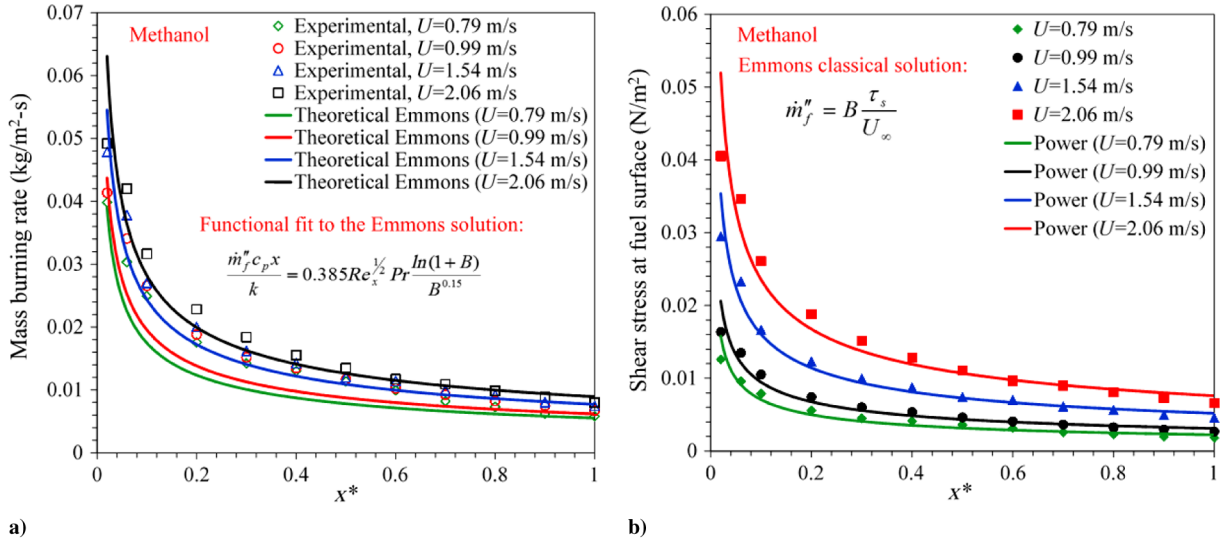

a) b)

Fig. 7 Depiction of a) variation of local mass burning rates along the fuel surface length; and b) distribution of shear stress at fuel surface for different values of U_∞.

13.47, 14.56, and 15.96 g/m^{2}s for $U_\infty = 0.79$, 0.99, 1.54, and 2.06 m/s, respectively, using Eq. (2). Appropriate average values of transport properties were used to calculate the constant C in Eq. (2) and are given in Table 1 [33,34]. It is to be noted that we evaluated the transport properties following the work of Kim et al. [3], in which they evaluated the value of k at the wall and the value of c_p at the adiabatic flame temperature of the given fuel. The assumption of a unity Prandtl number in deriving Eq. (2) also supports such selection of transport properties, because evaluation of the transport properties at the wall, namely, μ_w and k_w, and evaluation of the specific heat at the adiabatic flame temperature of the given fuel results in a unity Prandtl number. Choosing the transport properties as outlined earlier works well in estimating the average mass burning rates for methanol diffusion flames established under different forced-flow conditions. The average mass burning rate evaluated though the load cell data was found to be 12.14, 12.48, 13.41, and 14.69 g/m^{2}s for $U_\infty =$ 0.79, 0.99, 1.54, and 2.06 m/s, respectively. The error in the estimation of the average mass burning rate was therefore found to be +1.98, +7.93, +8.57, and +8.65% for $U_\infty = 0.79$, 0.99, 1.54, and 2.06 m/s, respectively.

D. Local Mass Burning Rates and Shear Stress at Fuel Surface

Figure 7a also shows the variation of the local mass burning rate for methanol diffusion flames, using the theoretical correlation from Eq. (2) and the nondimensional temperature gradients at the condensed fuel surface. Because of the availability of fresh oxidizer, higher convective heat feedback, higher temperature gradients, and lower standoff distances near the leading edge, the local burning rate is highest here and subsequently decreases as we move downstream toward the trailing edge. The burning rate decreases, due to the lack of fresh oxidizer, lower convective heat feedback, lower temperature gradients, and higher flame standoff distances as we move downstream. Also, the local mass burning rate for a methanol boundary-layer diffusion flame is almost proportional to $x^{-0.5}$, confirming the power law relationship for laminar forced-convective burning on a horizontal surface [1]. The local mass burning rate evaluated by using Eq. (2) was also compared against the theoretical mass burning rate given by Emmons [1]. Emmons [1] carried out an exact analysis for forced convection burning of a flat plate following the well-known Blasius solution for incompressible flow. Glassman [35] presents a functional fit to the Emmons solution as

$$\frac{\dot{m}_f'' c_p x}{k} = 0.385\left(\frac{U_\infty x}{\nu_\infty}\right)^{1/2} Pr \frac{\ell_n(1+B)}{B^{0.15}} \tag{4}$$

where k represents the thermal conductivity of the gas phase, c_p the specific heat of the gas phase, Pr the Prandtl number, B the mass transfer number, U_∞ the freestream velocity, ν_∞ the kinematic viscosity of the gas phase, and x the coordinate parallel to the fuel surface. The close agreement between the theoretical and experimental local mass burning rates suggests that the proposed correlation works quite well in estimating the local mass burning rates for forced-convective boundary-layer diffusion flames as well.

Emmons [1] also hypothesized that the rate of fuel evaporation, and hence the rate of burning either in the boundary layer or in the wake behind the body, is related to the shear stress by

$$\dot{m}_f'' = B\frac{\tau_s}{U_\infty} \tag{5}$$

With the knowledge of local mass burning rates using Eq. (2), the shear stress at the fuel surface can be effectively calculated. Thus, the combustion rate in the boundary layer on a flat plate is simply related to the velocity gradient at the surface. Shear stress at the fuel surface follows the same power law dependence with streamwise distance x as that of the local mass burning rate and can be used to calculate the friction coefficient C_f, which can be expressed as

$$C_f = \frac{\tau_s}{(1/2)\rho_\infty U_\infty^2} \tag{6}$$

Figure 7b shows the shear stress distribution at the fuel surface for a methanol boundary-layer diffusion flame for $U_\infty = 0.79, 0.99, 1.54,$ and 2.06 m/s, respectively.

Table 1 Physical properties

Properties	Methanol
Mass transfer number B	2.5 [33]
Thermal conductivity k_w (W/$m \cdot$ K) evaluated at pyrolyzing wall temperature	0.028 [34]
Specific heat c_p evaluated at adiabatic flame temperature	1394.5 [34]
$T_{w,p}$, K	337 [33]
$T_{\text{fl,ad}}$, K	2150 [34]
Length of the condensed fuel surface L, m	0.10

E. Wall Heat Fluxes in the Pyrolysis Zone

Using gas-phase temperature measurements and local mass burning rates, heat fluxes were evaluated in the pyrolysis zone at various streamwise locations along the condensed fuel surface. Reasonable approximations were made to simplify the heat balance analysis. The fuel surface was assumed to be opaque with an emissivity and absorptivity of unity. The surface radiative heat loss was given with respect

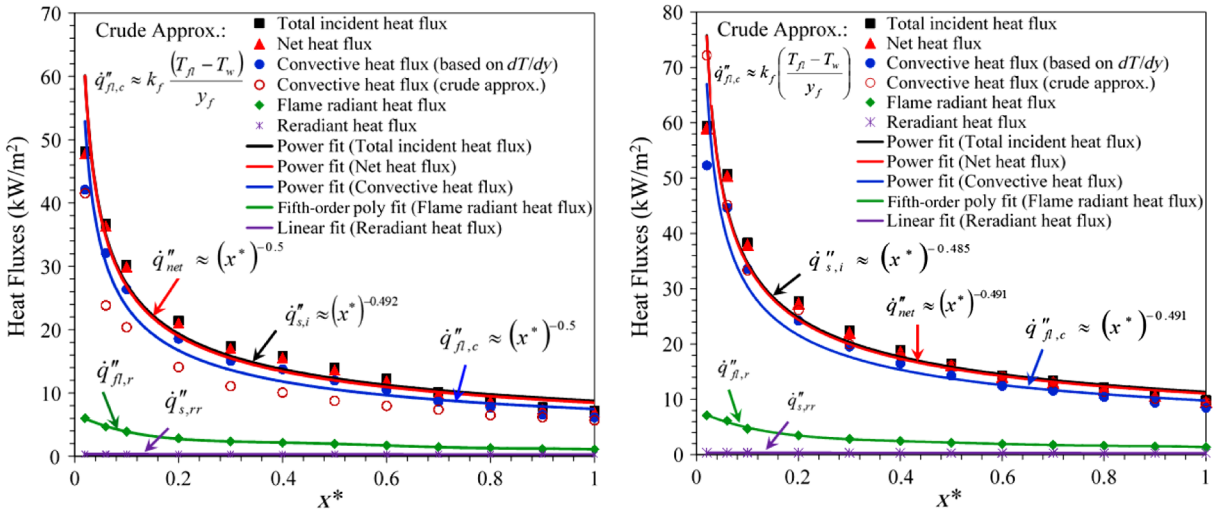

Fig. 8 Distribution of various components of flame heat flux in pyrolysis zone for methanol boundary-layer diffusion flame at (left) $U_\infty = 0.79$ and (right) 2.06 m/s.

to T_∞. The energy balance at the condensed fuel surface ($y = 0$) for steady burning of liquid fuels becomes

$$\dot{m}_f'' L_v = \dot{q}_{\mathrm{fl},c}'' + \dot{q}_{\mathrm{fl},r}'' - \dot{q}_{s,\mathrm{rr}}'' \tag{7}$$

and

$$\dot{m}_f'' L_v = k_w \left(\frac{\partial T}{\partial y}\right)_{y=0} + \dot{q}_{\mathrm{fl},r}'' - \sigma(T_w^4 - T_\infty^4) \tag{8}$$

where $\dot{q}_{\mathrm{fl},c}''$, $\dot{q}_{\mathrm{fl},r}''$, $\dot{q}_{s,\mathrm{rr}}''$, and L_v represent the convective heat flux, radiative heat flux, reradiation heat flux from the surface, and effective heat of gasification or vaporization, respectively. Here, the convective heat flux is measured by using the expression $k_w(\partial T/\partial y)_{y=0}$, which represents the gas-phase convective heating [33]. The flame imparts heat feedback to the condensed fuel surface primarily in two modes: convective and radiative. For convective-dominated steady burning, the convective heat flux from the flame is equal to $k_w(\partial T/\partial y)_{y=0}$ at the condensed fuel surface [33]. Therefore, the convective heat flux from the flame is equal to the conductive heat flux at the fuel surface for convective-dominated steady burning.

For a boundary-layer diffusion flame, the convective heat flux can be further approximated as [33]

$$\dot{q}_{\mathrm{fl},c}'' \approx h(T_{\mathrm{fl}} - T_w) \approx \frac{k_f(T_{\mathrm{fl}} - T_w)}{y_f} \tag{9}$$

where

$$h \approx \frac{k_f}{y_f} \tag{10}$$

This crude approximation allows us to calculate the convective flux in boundary-layer diffusion flames by estimating the wall T_w and flame temperatures T_{fl} at various streamwise locations along the pyrolysis zone together with knowledge of flame standoff distances y_f. In the preceding equation, k_f is the thermal conductivity of the gas phase evaluated at a mean film temperature (preferably mean of the actual flame and wall temperatures). To calculate convective fluxes by using Eq. (9), it is very important that flame and wall temperatures must be accurately determined along with precise measurements of flame standoff distances. Errors in estimating k_f, y_f, T_{fl}, and T_w could lead to serious deviations in estimating convective heat fluxes by using Eq. (9). However, using temperature gradients at the fuel surface is the most accurate way to evaluate the convective heat flux and will be compared with this crude approximation.

The reradiation heat flux from the surface $\dot{q}_{s,\mathrm{rr}}''$ can be evaluated by knowledge of the wall and ambient temperatures, respectively. Using the theoretical correlation in Eq. (2), the net heat flux $\dot{q}_{\mathrm{net}}''$ ($\dot{q}_{\mathrm{net}}'' = \dot{m}_f'' L_v$) can be estimated at various streamwise locations along the pyrolysis zone simply by the knowledge of local mass burning rates along the condensed fuel surface. The effective heat of gasification or vaporization was taken to be 1.2 kJ/g for methanol [33]. The radiative heat flux $\dot{q}_{\mathrm{fl},r}''$ can then easily be computed by using Eq. (8). Even if we take into account the nonunity absorptivity of the real surface, the incident radiant heat flux calculated would not vary much due to the low proportion of radiant emissions in these small fires. For larger or sootier flames, a more precise treatment of the fuel surface properties may be required. The total heat flux incident to the surface $\dot{q}_{s,i}''$ can then be defined as the sum of the convective and radiative components of the flame heat flux. Figure 8 shows the various components of flame heat flux in the pyrolysis zone of a methanol diffusion flame at $U_\infty = 0.79$ and 2.06 m/s.

Based on these results, the convective heat flux is relatively high and contributes approximately 86% of the total heat flux. The net heat feedback to the condensed fuel surface is the sum of the convective and radiative components minus reradiation from the surface. Thus, convection is the dominant mode of heat transfer and radiative contributions are small. This is reasonable for the small laminar flames studied here. With knowledge of the local distribution of various components of heat flux, one can further compute the average value of the given components by using

$$\dot{q}_{\mathrm{avg}}'' = \left(\frac{1}{L}\right) \int_0^L \dot{q}'' \, \mathrm{d}x \tag{11}$$

The average total incident heat flux from the flame to the wall was estimated to be 15.18 and 19.50 kW/m^2 for $U_\infty = 0.79$ and 2.06 m/s, respectively. The average convective heat flux from the flame to the wall was estimated to be 13.09 and 16.97 kW/m^2 for $U_\infty = 0.79$ and 2.06 m/s, respectively. The average radiative heat feedback from the flame was then calculated to be 2.09 and 2.53 kW/m^2, respectively for $U_\infty = 0.79$ and 2.06 m/s. Thus, convection is the dominant mode of heat transfer in steady laminar boundary-layer diffusion flames and is primarily responsible for the pyrolysis of fuel. Also, convective and total incident heat flux to the condensed fuel surface increases as the freestream velocity increases. This results in higher burning rates at higher freestream velocities.

V. Conclusions

The gas-phase temperature profiles across a laminar boundary-layer diffusion flame established over a methanol condensed fuel

surface were measured for four different incoming flow velocities. The results suggest that local mass burning rates can be obtained from these measurements by using a theoretical correlation that is based on the Reynolds analogy. The given methodology works well for both free- and forced-convective boundary-layer diffusion flames and is capable of giving reasonable estimates of local mass burning rates and heat fluxes in such flames. With the knowledge of local mass burning rates, shear stress and hence the strain rates at the condensed fuel surface can be easily obtained. Flame stability mechanisms can thus be studied in more detail with the knowledge of these local properties. Convective heat flux was found to be the dominant mode of heat transfer in these small laminar flames and accounted for nearly 86% of the total incident heat flux. At the condensed fuel surface, total incident heat flux was found to increase with the freestream air velocity. This results in higher burning rates at higher freestream air velocities. Although the initial study was taken in the laminar regime, further extensions of the technique could be applicable to turbulent boundary-layer combustion in propulsion-oriented research.

Appendix: A Thermocouple Corrections

A1 Radiation Correction for the Thermocouple

The temperature measurements reported in this study have been corrected for thermocouple radiation. Flame temperature measurements across the width of the fuel sample showed no significant variation, except near the edges. Therefore, thermocouples at the center of the flame were used to produce a map of temperatures in the boundary layer by moving it across the flame (y direction) and along the length of the flame (x direction). Two thermocouples (50 and 75 μm wire diameter) were traversed along the same path at the center of the flame for accurate radiation corrections. All temperature measurements reported in this paper are an average of at least five independent tests conducted under the same conditions. In the most general case, an energy balance on the thermocouple junction takes the following form:

$$\dot{Q}_{\text{cat}} + \dot{Q}_{\text{conv}} + \dot{Q}_{\text{rad}} + \dot{Q}_{\text{cond}} = m_{\text{tc}} c_p \frac{\mathrm{d}T_{\text{tc}}}{\mathrm{d}t} \tag{A1}$$

with heat transfer associated with surface-induced catalytic reactions, convection between the gases and the thermocouple, radiant heat transfer between the thermocouple and its surroundings, conduction along the thermocouple wires, and transient heating or cooling of the thermocouple incorporated in Eq. (A1). The thermocouple junction properties that characterize the transient term in the preceding expression include the mass of the thermocouple junction m_{tc} and the specific heat c_p. For transient measurements, the convection and thermal inertia terms are both important, in addition to radiation. Neglecting the conduction error and errors due to catalytic effects [Eq. (A1)] reduces to the following form for transient measurements:

$$(T_g - T_{\text{tc}}) = \frac{m_{\text{tc}} c_p}{h A_{\text{tc}}} \frac{\mathrm{d}T_{\text{tc}}}{\mathrm{d}t} + \frac{\varepsilon_{\text{tc}} \sigma}{h} (T_{\text{tc}}^4 - T_{\text{surr}}^4) \tag{A2}$$

$$(T_g - T_{\text{tc}}) = \tau \frac{\mathrm{d}T_{\text{tc}}}{\mathrm{d}t} + \frac{\varepsilon_{\text{tc}} \sigma}{h} (T_{\text{tc}}^4 - T_{\text{surr}}^4) \tag{A3}$$

where τ is the characteristic response time or time constant of the thermocouple. Equation (A3) shows that the time constant of the thermocouple is not only related to the physical properties of the thermocouple (i.e., the mass of the thermocouple junction m_{tc}, the specific heat c_p, and the surface area of the junction A_{tc}), but also depends on heat transfer coefficient of the flow h. There is a substantial body of literature devoted to the measurement of time constant of the thermocouple [36–41].

For steady-state measurements, as in our case, Eq. (A1) reduces to a convective–radiative heat balance (neglecting the conduction error and errors due to catalytic effects), given by

$$h(T_g - T_{\text{tc}}) = \varepsilon_{\text{tc}} \sigma (T_{\text{tc}}^4 - T_{\text{surr}}^4) \tag{A4}$$

$$(T_g - T_{\text{tc}}) = \frac{\varepsilon_{\text{tc}} \mathrm{d}_w \sigma}{kNu} (T_{\text{tc}}^4 - T_{\text{surr}}^4) \tag{A5}$$

where T_g is the real gas temperature, T_{tc} is the thermocouple junction (or bead) temperature, T_{surr} is the temperature of the surroundings, ε_{tc} is the emissivity of the thermocouple junction, σ is the Stefan–Boltzmann constant, and h is the convective heat transfer coefficient of the flow over the thermocouple junction defined as $h = kNu/\mathrm{d}_w$. Nu is the Nusselt number, k is the thermal conductivity of the gas, and d_w is the thermocouple wire diameter. The choice of the Nusselt number correlation is of paramount importance in calculating a radiation correction to the measured thermocouple temperature because, as shown in Eq. (A5), the radiation correction is inversely proportional to the Nusselt number. This choice is complicated, however, due to the existence of multiple "appropriate" Nusselt number correlations and the difficulty in estimation of the properties of the gas mixture surrounding the thermocouple, particularly its thermal conductivity. The bulk of evidence in literature, however, clearly indicates that a cylindrical Nusselt number correlation is most appropriate for describing the convective heat transfer to nearly all practical thermocouples [42], preferably that of Collis and Williams [25]. A commonly used expression from Collis and Williams can be written as [25]

$$Nu\left(\frac{T_m}{T_g}\right)^{-0.17} = 0.24 + 0.56 Re_{d_w}^{0.45} = 0.24 + 0.56\left(\frac{U \mathrm{d}_w}{\nu}\right)^{0.45} \tag{A6}$$

which was obtained for $0.02 < Re < 44$, with the Reynolds number evaluated at the so-called film temperature, T_m, which is the mean of the thermocouple and freestream temperatures [i.e., $0.5(T_g + T_{\text{tc}})$]. Here, the Reynolds number Re is defined as indicated for the local gas flow velocity U and kinematic viscosity v. Substituting Eq. (A6) into Eq. (A5) and neglecting the small temperature dependence in Eq. (A6), we have a system of two equations with two unknowns (namely, T_g and U):

$$T_g - T_{\text{tc}_1} = \frac{\varepsilon_{\text{tc}_1} \mathrm{d}_{w_1} \sigma}{k[0.24 + 0.56(U d_{w_1}/\nu)^{0.45}]} (T_{\text{tc}_1}^4 - T_{\text{surr}}^4) \tag{A7}$$

and

$$T_g - T_{\text{tc}_2} = \frac{\varepsilon_{\text{tc}_2} \mathrm{d}_{w_2} \sigma}{k[0.24 + 0.56(U \mathrm{d}_{w_2}/\nu)^{0.45}]} (T_{\text{tc}_2}^4 - T_{\text{surr}}^4) \tag{A8}$$

which demonstrates that the difference between a thermocouple reading and the actual gas temperature (i.e., the error in gas temperature measurement) increases for larger diameter thermocouples, whereas it is reduced by increasing the gas flow velocity over the junction. In solving the preceding equations, iteration is required because the gas conductivity and kinematic viscosity are functions of the gas temperature. Initially, the gas temperature is taken to be the bead temperature for the purpose of evaluating the thermal conductivity and kinematic viscosity; then, the approximate value of the gas temperature is used to reevaluate the thermal conductivity and viscosity.

The emissivity of the bead ε_{tc} can also be found as a function of its temperature. In an analysis outlined by Jakob [29], Maxwell's wave equations can be solved to yield the complex indices of refraction for a metal as a function of its electrical resistivity. In the limit of low resistivity and assuming a large index of refraction, which is true for metals, Jakob [29] gives the hemispherical total emissivity of platinum Pt as

$$\epsilon = 0.751(r_e T)^{1/2} - 0.396(r_e T), \qquad 0 < r_e T < 0.2 \tag{A9}$$

where, for platinum, $r_e = r_{e,273} T/273$, with T in Kelvin and $r_{e,273} = 11 \times 10^{-6} \Omega$ cm [43]. Therefore, the platinum emissivity becomes

$$\epsilon = 1.507 \times 10^{-4} T - 1.596 \times 10^{-8} T^2 \qquad \text{(A10)}$$

for $0 < T < 2230$ K. This equation is also confirmed by comparison with experimental data [30]. It was shown [30] that, for temperatures where radiation is important, predicted and observed emissivities agree to within 1%. The emissivity of the thermocouple bead or junction can therefore be evaluated by using the preceding expression. Note that iteration is not needed for the evaluation of the platinum emissivity, because this property is a function of the junction or bead temperature, which is known.

The actual gas temperature can then be evaluated by solving Eqs. (A7) and (A8). During experiments, the two thermocouples were traversed exactly to the same measurement points and data were sampled to account for radiation correction in the temperature measurements.

A2 Conduction Correction for the Thermocouple

Rapid thermal conduction along thermocouple wires can result in significant heat loss from the thermocouple wire and junction to the larger, cooler lead wires or support (cooler on account of increased radiation and conductive losses through the thermocouple support structure). However, this mechanism of heat loss from the thermocouple is usually avoidable through the use of sufficiently long and thin thermocouple wires on both sides of the junction. According to Bradley and Matthews [44], the conduction heat loss is assumed to be negligible if $l > 200\, d_w$, where l is the length of the fine wire. However, a more detailed analysis by Petit et al. [45] reveals that a better criterion is to use wires of length l such that $l/l_c > 10$, in which l_c is the characteristic length, defined as

$$l_c = \sqrt{\frac{k_w d_w}{4 h_{\text{conv}}}} \qquad \text{(A11)}$$

This criterion accounts for both the characteristics of the flow and of the sensor. Values obtained from applying Petit criterion to the thermocouples used in this study, with the exposed wire of 10 mm length and wire diameter of 50 μm at different locations in and out of the flame, were found to be in the range of 14–17 for the l/l_c ratio, which is above the recommended value of 10. Overall, the conduction error is considered negligible in this study.

Acknowledgments

The authors would like to acknowledge financial support for this work from the Minta Martin Foundation at the University of Maryland, College Park.

References

[1] Emmons, H., "The Film Combustion of Liquid Fuel," *Zeitschrift für Angewandte Mathematik und Mechanik*, Vol. 36, Nos. 1–2, 1956, pp. 60–71. doi:10.1002/zamm.19560360105

[2] Kosdon, F. J., Williams, F. A., and Buman, C., "Combustion of Vertical Cellulosic Cylinders in Air," *Proceedings of the Combustion Institute*, Vol. 12, No. 1, 1969, pp. 253–264. doi:10.1016/S0082-0784(69)80408-X

[3] Kim, J., de Ris, J., and Kroesser, F., "Laminar Free-Convective Burning of Fuel Surfaces," *Proceedings of the Combustion Institute*, Vol. 13, No. 1, 1971, pp. 949–961. doi:10.1016/S0082-0784(71)80095-4

[4] Hirano, T., Iwai, K., and Kanno, Y., "Measurement of Velocity Distribution in Boundary-Layer over a Flat Plate with a Diffusion Flame," *Astronautica Acta*, Vol. 17, Nos. 4–5, 1972, p. 811.

[5] Hirano, T., and Kanno, Y., "Aerodynamic and Thermal Structures of the Laminar Boundary Layer over a Flat Plate with a Diffusion Flame," *Proceedings of the Combustion Institute*, Vol. 14, No. 1, 1973, pp. 391–398. doi:10.1016/S0082-0784(73)80038-4

[6] Pagni, P., and Shih, T., "Excess Pyrolyzate," *Proceedings of the Combustion Institute*, Vol. 16, No. 1, 1977, pp. 1329–1343. doi:10.1016/S0082-0784(77)80419-0

[7] Ahmad, T., and Faeth, G. M., "Turbulent Wall Fires," *Proceedings of the Combustion Institute*, Vol. 17, No. 1, 1979, pp. 1149–1160. doi:10.1016/S0082-0784(79)80109-5

[8] Annamalai, K., and Sibulkin, M., "Flame Spread over Combustible Surfaces for Laminar Flow Systems Part I: Excess Fuel and Heat Flux," *Combustion Science and Technology*, Vol. 19, Nos. 5–6, 1979, pp. 167–183. doi:10.1080/00102207908946878

[9] Andreussi, P., and Petarca, L., "Film Combustion of Ethyl Alcohol in a Parallel Air Stream," *Proceedings of the Combustion Institute*, Vol. 18, No. 1, 1981, pp. 1861–1869. doi:10.1016/S0082-0784(81)80192-0

[10] Singh, A. V., and Gollner, M. J., "Estimation of Local Mass Burning Rates for Steady Laminar Boundary Layer Diffusion Flames," *Proceedings of the Combustion Institute*, Vol. 35, No. 3, 2015, pp. 2527–2534. doi:10.1016/j.proci.2014.05.040

[11] Singh, A. V., and Gollner, M. J., "A Methodology for Estimation of Local Heat Fluxes in Steady Laminar Boundary Layer Diffusion Flames," *Combustion and Flame*, Vol. 162, No. 5, 2015, pp. 2214–2230. doi:10.1016/j.combustflame.2015.01.019

[12] Chilton, T. H., and Colburn, A. P., "Mass Transfer (Absorption) Coefficients Prediction from Data on Heat Transfer and Fluid Friction," *Industrial and Engineering Chemistry*, Vol. 26, No. 11, 1934, pp. 1183–1187. doi:10.1021/ie50299a012

[13] Silver, R., "Application of the Reynolds Analogy to Combustion of Solid Fuels," *Nature*, Vol. 165, May 1950, pp. 725–726. doi:10.1038/165725a0

[14] Spalding, D., "Combustion of Liquid Fuel in Gas Stream," *Fuel*, Vol. 29, No. 1, 1950, pp. 2–7.

[15] Burke, S., and Schumann, T., "Diffusion Flames," *Proceedings of the Combustion Institute*, Vols. 1–2, 1948, pp. 2–11. doi:10.1016/S1062-2888(65)80003-X

[16] Spalding, D. B., "The Combustion of Liquid Fuels," *Proceedings of the Combustion Institute*, Vol. 4, No. 1, 1953, pp. 847–864. doi:10.1016/S0082-0784(53)80110-4

[17] Pagni, P. J., "Diffusion Flame Analyses," *Fire Safety Journal*, Vol. 3, No. 4, 1981, pp. 273–285. doi:10.1016/0379-7112(81)90049-7

[18] Torero, J. L., Vietoris, T., Legros, G., and Joulain, P., "Estimation of a Total Mass Transfer Number from the Standoff Distance of a Spreading Flame," *Combustion Science and Technology*, Vol. 174, Nos. 11–12, 2002, pp. 187–203. doi:10.1080/713712953

[19] Sirignano, W., "Theory of Flame Spread Above Solids," *Acta Astronautica*, Vol. 1, Nos. 9–10, 1974, pp. 1285–1299. doi:10.1016/0094-5765(74)90052-6

[20] Williams, F. A., "Mechanisms of Fire Spread," *Proceedings of the Combustion Institute*, Vol. 16, No. 1, 1977, pp. 1281–1294. doi:10.1016/S0082-0784(77)80415-3

[21] Hirano, T., and Kinoshita, M., "Gas Velocity and Temperature Profiles of a Diffusion Flame Stabilized in the Stream over Liquid Fuel," *Proceedings of the Combustion Institute*, Vol. 15, No. 1, 1975, pp. 379–387. doi:10.1016/S0082-0784(75)80312-2

[22] Andreussi, P., "Modelling of Laminar Diffusion Flames over a Horizontal Plate," *Combustion and Flame*, Vol. 45, 1982, pp. 1–6. doi:10.1016/0010-2180(82)90027-X

[23] Andreotti, S., Andreussi, P., and Petarca, L., "Boundary Layer Burning of Fuel Surfaces: Thermal and Aerodynamic Structure of the Flame," *Combustion Science and Technology*, Vol. 40, Nos. 5–6, 1984, pp. 279–291. doi:10.1080/00102208408923811

[24] Ha, J. S., Shim, S. H., and Shin, H. D., "Boundary Layer Diffusion Flame over a Flat Plate in the Presence and Absence of Flow Separation," *Combustion Science and Technology*, Vol. 75, Nos. 4–6, 1991, pp. 241–260. doi:10.1080/00102209108924091

[25] Collis, D., and Williams, M., "Two-Dimensional Convection from Heated Wires at Low Reynolds Numbers," *Journal of Fluid Mechanics*, Vol. 6, No. 3, 1959, pp. 357–384. doi:10.1017/S0022112059000696

[26] Du Plessis, M., Wang, R., and Kahawita, R., "Investigation of the Near-Region of a Square Jet," *Journal of Fluids Engineering*, Vol. 96, No. 3, 1974, pp. 246–251. doi:10.1115/1.3447147

[27] Sfeir, A., "The Velocity and Temperature Fields of Rectangular Jets," *International Journal of Heat and Mass Transfer*, Vol. 19, No. 11, 1976,

pp. 1289–1297.
doi:10.1016/0017-9310(76)90081-8
[28] Sforza, P., Steiger, M., and Trentacoste, N., "Studies on Three-Dimensional Viscous Jets," *AIAA Journal*, Vol. 4, No. 5, 1966, pp. 800–806.
doi:10.2514/3.3549
[29] Jakob, L. M., *Heat Transfer*, Vol. 1, Wiley, New York, 1967.
[30] Gubareff, G., Janssen, J., and Torborg, R., *Thermal Radiation Properties Survey, 2nd, Minneapolis: Minneapolis-Honeywell Regulator Company*, Honeywell Research Center, Minneapolis, MN, 1960.
[31] Raghavan, V., Rangwala, A., and Torero, J., "Laminar Flame Propagation on a Horizontal Fuel Surface: Verification of Classical Emmons Solution," *Combustion Theory and Modelling*, Vol. 13, No. 1, 2009, pp. 121–141.
doi:10.1080/13647830802483729
[32] Incropera, F. P., *Fundamentals of Heat and Mass Transfer*, John Wiley & Sons, Hoboken, NJ, 2011.
[33] Quintiere, J. G., *Fundamentals of Fire Phenomena*, John Wiley & Sons, England, 2006.
[34] Turns, S., *Introduction to Combustion*, Vol. 287, McGraw–Hill, New York, 1996.
[35] Glassman, I., *Combustion*, Academic Press, New York, 1997.
[36] Lockwood, F., and Odidi, A., "Measurement of Mean and Fluctuating Temperature and of Ion Concentration in Round Free-Jet Turbulent Diffusion and Premixed Flames," *Proceedings of the Combustion Institute*, Vol. 15, No. 1, 1975, pp. 561–571.
doi:10.1016/S0082-0784(75)80328-6
[37] Ballantyne, A., and Moss, J., "Fine Wire Thermocouple Measurements of Fluctuating Temperature," *Combustion Science and Technology*, Vol. 17, Nos. 1–2, 1977, pp. 63–72.
doi:10.1080/00102209708946813
[38] Miles, P., and Gouldin, F., "Determination of the Time Constant of Fine-Wire Thermocouples for Compensated Temperature Measurements in Premixed Turbulent Flames," *Combustion Science and Technology*, Vol. 89, Nos. 1–4, 1993, pp. 181–199.
doi:10.1080/00102209308924108
[39] Yule, A., Taylor, D., and Chigier, N., "Thermocouple Signal Processing and Online Digital Compensation," *Journal of Energy*, Vol. 2, No. 4, 1978, pp. 223–231.
doi:10.2514/3.62378
[40] Singh, A. V., Yu, M., Gupta, A. K., and Bryden, K. M., "Thermo-Acoustic Behavior of a Swirl Stabilized Diffusion Flame with Heterogeneous Sensors," *Applied Energy*, Vol. 106, June 2013, pp. 1–16.
doi:10.1016/j.apenergy.2013.01.044
[41] Singh, A. V., Eshaghi, A., Yu, M., Gupta, A. K., and Bryden, K. M., "Simultaneous Time-Resolved Fluctuating Temperature and Acoustic Pressure Field Measurements in a Premixed Swirl Flame," *Applied Energy*, Vol. 115, Feb. 2014, pp. 116–127.
doi:10.1016/j.apenergy.2013.10.058
[42] Shaddix, C. R., "Correcting Thermocouple Measurements for Radiation Loss—A Critical Review," *33rd National Heat Transfer Conference*, No. CONF-990805, Sandia National Lab., Livermore, CA, 1999.
[43] Hodgman, C. D., Weast, R. C., and Selby, S. M., *Handbook of Chemistry and Physics: A Ready-Reference Book of Chemical and Physical Data*, 40th ed., Chemical Rubber Publ. Co., Cleveland, OH, 1961.
[44] Bradley, D., and Matthews, K., "Measurement of High Gas Temperatures with Fine Wire Thermocouples," *Journal of Mechanical Engineering Science*, Vol. 10, No. 4, 1968, pp. 299–305.
doi:10.1243/JMES_JOUR_1968_010_048_02
[45] Petit, C., Gajan, P., Lecordier, J.-C., and Paranthoen, P., "Frequency Response of Fine Wire Thermocouple," *Journal of Physics E: Scientific Instruments*, Vol. 15, No. 7, 1982, p. 760.
doi:10.1088/0022-3735/15/7/017

R. Lucht
Associate Editor